

REPORT DOCUMENTATION PAGE				Form Approved OMB No. 0704-0188	
Public reporting burden for this collection of information is estimated to average 1 hour per response, including the time for reviewing instructions, searching existing data sources, gathering and maintaining the data needed, and completing and reviewing the collection of information. Send comments regarding this burden estimate or any other aspect of this collection of information, including suggestions for reducing the burden, to Department of Defense, Washington Headquarters Services, Directorate for Information Operations and Reports (0704-0188), 1215 Jefferson Davis Highway, Suite 1204, Arlington, VA 22202-4302. Respondents should be aware that notwithstanding any other provision of law, no person shall be subject to any penalty for failing to comply with a collection of information if it does not display a currently valid OMB control number. PLEASE DO NOT RETURN YOUR FORM TO THE ABOVE ADDRESS.					
1. REPORT DATE (DD-MM-YYYY) 15-07-2003		2. REPORT TYPE Final Report		3. DATES COVERED (From - To) 11 July 2001 - 11-Jul-02	
4. TITLE AND SUBTITLE <div style="text-align: center; font-size: 1.2em;">Experiments on Coupled Josephson Junction Devices</div>			5a. CONTRACT NUMBER F61775-01-WE045		
			5b. GRANT NUMBER		
			5c. PROGRAM ELEMENT NUMBER		
6. AUTHOR(S) A. A. Abdumalikov and A. V. Ustinov			5d. PROJECT NUMBER		
			5d. TASK NUMBER		
			5e. WORK UNIT NUMBER		
7. PERFORMING ORGANIZATION NAME(S) AND ADDRESS(ES) University of Erlangen-Nuremberg Erwin-Rommel-Str. 1 Erlangen 91058 Germany				8. PERFORMING ORGANIZATION REPORT NUMBER <div style="text-align: center;">N/A</div>	
9. SPONSORING/MONITORING AGENCY NAME(S) AND ADDRESS(ES) EOARD PSC 802 BOX 14 FPO 09499-0014				10. SPONSOR/MONITOR'S ACRONYM(S)	
				11. SPONSOR/MONITOR'S REPORT NUMBER(S) SPC 01-4045	
12. DISTRIBUTION/AVAILABILITY STATEMENT Approved for public release; distribution is unlimited. /					
20040625 146					
13. SUPPLEMENTARY NOTES					
14. ABSTRACT This report results from a contract tasking University of Erlangen-Nuremberg as follows: The contractor will investigate coupled Josephson devices of two different kinds. First, the contractor will test a new concept of active antennas to couple radiation out from Josephson arrays. Using a mixed series-parallel array-biasing scheme, the contractor will design and perform waveguide-coupled emission experiments with single- and double-row arrays at 80-120 GHz. If successful, this scheme will be further implemented and tested using dipole antennas for the 400-500 GHz range. The contractor will also investigate the loop antenna array scheme as detailed in the technical proposal. The experiments will be done with Nb/Al-AOx/Nb Josephson junction arrays. The second Josephson device to be investigated (including design, fabrication, and testing) are novel q-bit devices. These q-bits are hoped to be more flexible and therefore more suitable hardware for quantum computing than single- loop SQUIDS currently pursued by other researcher groups. Full details are provided in the accompanying technical proposal.					
15. SUBJECT TERMS EOARD, Josephson junctions, terahertz electronics					
16. SECURITY CLASSIFICATION OF:			17. LIMITATION OF ABSTRACT UL	18. NUMBER OF PAGES 29	19a. NAME OF RESPONSIBLE PERSON Christopher E. Reuter, Ph. D.
a. REPORT UNCLAS	b. ABSTRACT UNCLAS	c. THIS PAGE UNCLAS			19b. TELEPHONE NUMBER (Include area code) +44 20 7514 4474

Final Report

Experiments on Coupled Josephson Junction Devices*

A. A. Abdumalikov and A. V. Ustinov

Physikalisches Institut III, Universität Erlangen-Nürnberg
D-91058 Erlangen, Germany

* Supported by European Office of Aerospace Research and Development (EOARD)
under Contract F61775-01-WE045

March 2003

Contents

Abstract	1
1 Series-parallel arrays	1
1 Layout 1	1
2 Measurements and discussion: Layout 1	2
3 Layout 2	4
4 Measurements and discussion: Layout 2	4
4.1 Sample C79#1	4
4.2 Sample C92#2	6
References	8
2 Full-wavelength loop antenna arrays	9
1 Loop antenna array	9
2 Measurements and discussion	9
3 Conclusion	13
References	14
3 Replacement of resistors by Josephson junctions in biasing leads	15
1 Introduction	15
2 Array layout	16
3 Experimental results	16
4 Conclusion	19
References	20
4 Triangular prism qubits	21
1 Introduction	21
2 Design	22
3 Experiment	22
4 Conclusion	24
References	25
5 Declarations	26

Abstract

In order to use effectively radiation from Josephson junctions Shitov has proposed a new design to couple them using a modified mixed series-parallel array-biasing scheme. We designed two different layouts of samples according to Shitov's proposal and performed dc measurements and radiation detection experiments at the frequency of 80 GHz. For the high temperature range we observed rather large radiation. Furthermore, we studied full wave length loop antenna arrays. The arrays with two cells have more complicated dynamics, similar to discrete rotobreathers in Josephson ladders. We have measured detailed current-voltage characteristics of single and double loop arrays with 4×3 , 4×4 , 4×5 , 4×6 and 4×7 junctions per cell in the broad temperature range between 4.2 K and 8 K. In order to decrease the space occupied by the arrays of Josephson junctions studied by us earlier, we replaced bias resistors by Josephson junctions. We designed a new set of arrays combining both the junction biasing and resistor biasing schemes on the same chip. The comparison of two alternative biasing schemes shows that the junction biasing introduces several unwanted complications in array characteristics. Finally, we report here our experimental study of novel qubit devices. The devices have been designed and fabricated using Nb-AlO_x-Nb technology. The read-out of qubit state has been performed by dc-SQUID. We observe clear signatures of coupling between the read-out SQUID and a qubit. The SQUID response has a hysteresis related to different states of the qubit.

Chapter 1

Series-parallel arrays

1 Layout 1

Mixed series-parallel Josephson junction arrays have been proposed by Jain et al [1] for high-frequency oscillators. Recently Shitov [2] suggested a modification of that scheme using microwave matching of dc bias leads. A sketch of such an array consisting of only 5 junctions is shown in Fig.1.

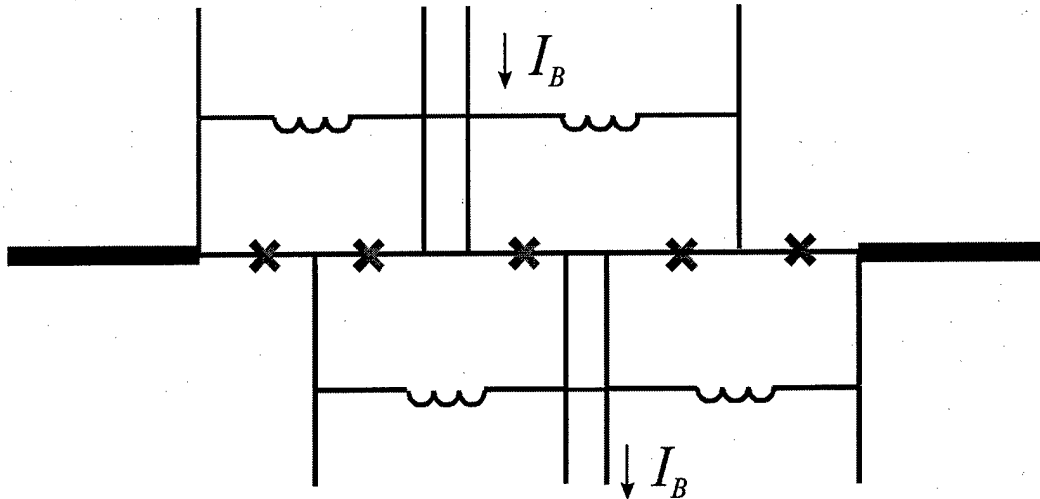


Figure 1.1: Series-parallel Josephson junction array scheme

The main idea of this layout is that Josephson junctions (indicated by crosses in Fig. 1.1) are arranged in parallel for DC current I_B applied to the array, while the AC voltages add up in series. The interference between the junctions can be tuned by the externally applied magnetic flux through the cells. At half frustration the amplitude of AC oscillations will be the largest as well as will be the radiation power. The DC component of the voltage across the dipole antenna attached to the edge junctions of the array should be equal to zero for even number of junctions and to a single junction voltage for odd number of junctions. The amplitude of AC voltage is expected to increase with the number of junctions. The array has to be operated in a resonant mode which frequency is determined by the cell inductance and junction capacitance.

2 Measurements and discussion: Layout 1

The samples according to our layout were prepared at the Hypres foundry. The size of each junction is $9\mu\text{m}^2$. The primary cell (containing 2 junctions and inductance) size is about $370\mu\text{m}^2$. The size of the adjacent (secondary) cell formed by the leads (vertical lines in Fig. 1.1) and lines which shorten them is about $2980\mu\text{m}^2$. We have designed arrays with 10 junctions and with 20 junctions. At the edges of the array we put capacitances equal to the capacitance of a junction. The arrays were designed to radiate in the range 95-105 GHz. However the radiation range was found to be shifted towards lower frequencies, because the critical current density, dielectric constant and other parameters came out slightly different then ones which were taken during the designing. In Fig. 1.2 we present the layout of the array of 20 junctions. The long side of the secondary cells is about a quarter wave length at the center frequency (100 GHz). This means that the loop at shorted one end will work as open at this frequency. The biasing leads of the array end with chock filters, which filter noise in the frequency range of 80-110 GHz. The edges of the array are attached to conductors that form a dipole antenna. This antenna also ends with chock filters. These filters are needed to prevent the leakage of the radiation outside a waveguide. The dipole antenna couples radiation to the waveguide.

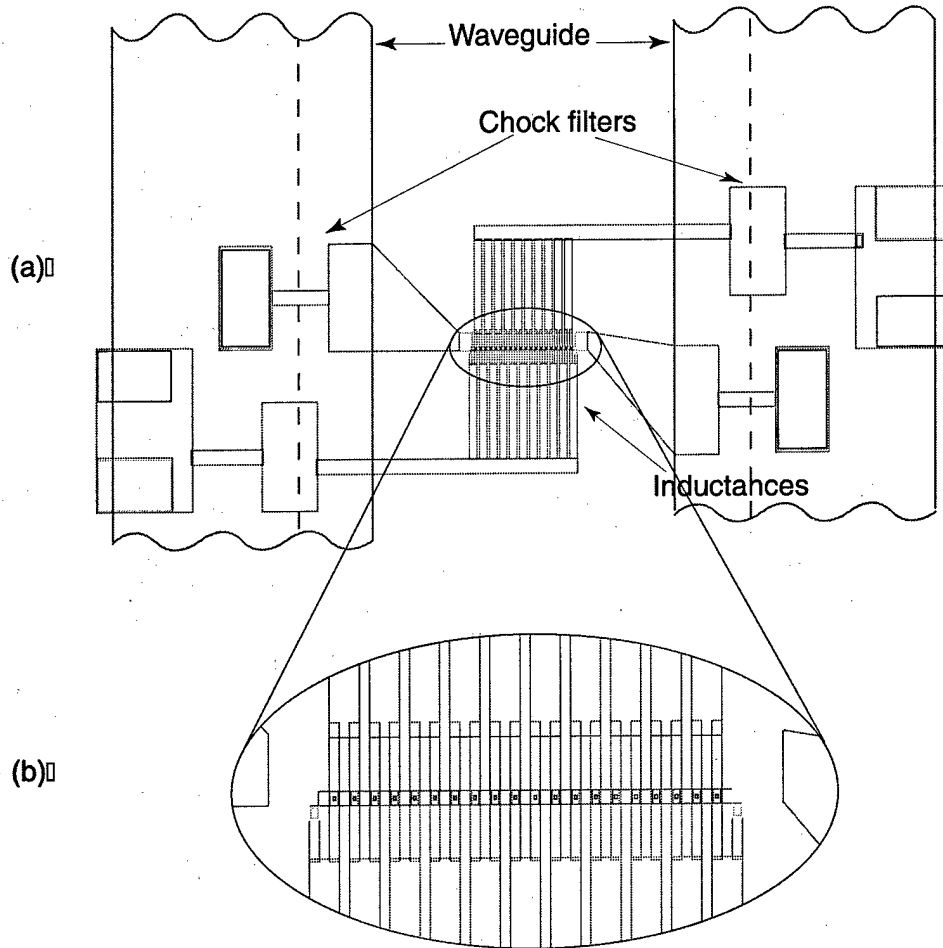


Figure 1.2: Layout of the array (a) and its enlarged junction area (b)

All measurements were done at $T \simeq 7$ K. The temperature was estimated from the gap voltage of the array, which was about 1.3 mV. To change the frustration through the array cell, a magnetic field perpendicular to the array's plane was used. As usual, first we did dc measurements of the current-voltage characteristics and $I_c(H)$ pattern. The I-V curve of the array with 10 junctions is shown in Fig. 1.3(a) by dots. This curve corresponds to the frustration through small cells of $f=0.4$. In the Fig. 1.3 the dependence of the critical current versus perpendicular magnetic field is presented. This curve does not look regular. We suppose that it is due to the large secondary cells, which are about eight times as large as the primary ones. However, it still shows sufficiently periodic behavior. In the presence of an external frustration in larger cells we may expect an additional supercurrent which brakes symmetry of the system. Moreover, during cooling down it is hard to avoid trapping random number of fluxons in larger cells. To eliminate this problem one can use resistive bridges instead of superconducting ones (green lines in Fig. 1.1), but in this case a considerable part of the AC current would dissipate on these resistors.

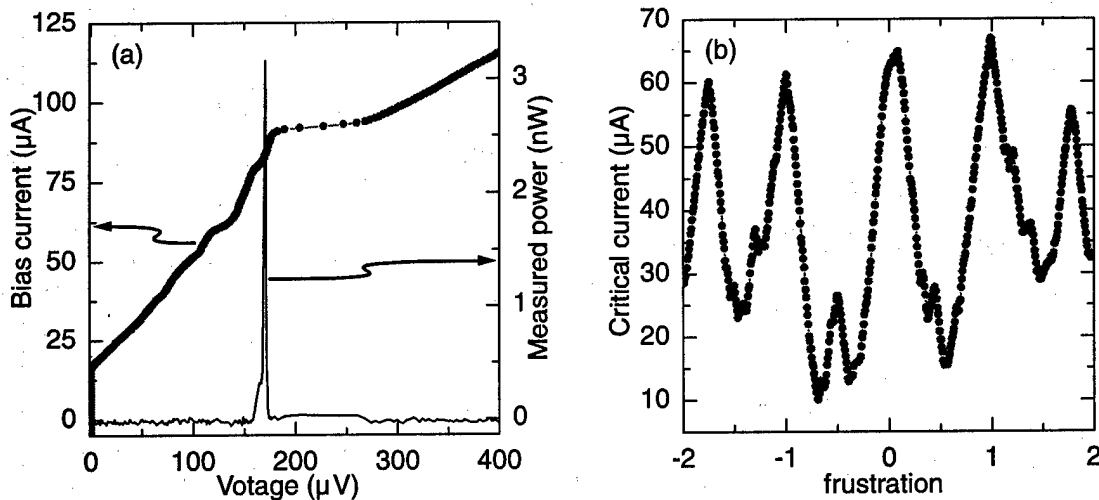


Figure 1.3: (a) Current voltage characteristics (dots) and measured radiation power (line) at 80 GHz; (b) critical current pattern versus perpendicular magnetic field.

From the I-V curve of the array one can see that there is a resonance at the voltage of about 180 μV . We have measured radiation from this array using our room temperature superheterodyne receiver. By black line in Fig. 1.3(a) we show the measured power dependence on voltage across the array for the presented I-V curve. On this curve, there is a very narrow peak at the same voltage as the resonance branch of the I-V curve.

The weak magnitude of the detected power can be partially explained by fault design of chock filters. All chock filters at the end of dipole antenna are also part of this antenna. As a part of the antenna they should be placed inside the waveguide. The waveguide position is shown in Fig. 1.2 by blue lines. In such position the bonding wires would be most probably working as RF shorts to the ground. In order to prevent this shorts, we had to make the waveguide's walls as thin as it is shown by dashed blue lines. This complication can be avoided by moving contact pads away from the waveguide walls.

Thus, in these experiments with Layout 1 the radiation was measured from all prepared samples. The detected radiation frequency is about 80 GHz. We note several design improvements to be made. First, we would have to avoid additional superconducting loops. The contact pads have to be placed away from the chock-filters.

3 Layout 2

In the Layout 2 we improved design of our series-parallel arrays. First improvement in this design is that we have interrupted the secondary superconducting loops by resistor bridges. The bias current now flows through the bias resistors. Second, the capacitors at the extremities of the array have been substituted by Josephson junctions. Finally, the contact pads have been moved away from the chock filters, so that the bonding wires do not anymore touch the waveguide.

4 Measurements and discussion: Layout 2

The samples according to our micro-layout were prepared at the Hypres foundry. The cell size of all prepared arrays is about $350 \mu\text{m}^2$. The length of the inductance leads is about $300 \mu\text{m}$. We have designed arrays with 10 and 22 junctions. The size of junctions was either $5 \times 5 \mu\text{m}^2$ or $3 \times 3 \mu\text{m}^2$. in order to decrease their McCumber parameter, the arrays have been measured in helium vapor at temperatures above 4.2 K. The actual measurement temperature was estimated from the gap voltage. Measurements with different arrays were done at slightly different temperatures. The parameters of the arrays and experimental data are summarized in Table 1.1.

Table 1.1: Parameters of the measured samples

Sample ID	Number of junctions	Junction size, μm^2	Critical current density, A/cm ²	Measurement temperature, K	Measured power level (a.u.)
C79#1	22	3x3	910	7.2	1.0
C79#2	22	5x5	910	7.5	0.2
C79#3	10	5x5	910	7.8	0.0
C92#1	22	3x3	970	7.8	0.0
C92#2	22	5x5	970	7.9	57.0

In order to change the frustration through the array cell, an external magnetic field perpendicular to the array's plane was used. As usual, first we did dc measurements of the current-voltage characteristics and $I_c(H)$ pattern. From dc measurements we estimate at which frequencies we the radiation may be expected. In the following we present measurement results for two arrays. Both arrays have the same number of junctions (22), but have different junction sizes.

4.1 Sample C79#1

The measurements with this array were done at $T=7.2$ K. The dc characteristics of the array are presented in Fig.1.4. The I-V curve is shown by dots in Fig. 1.4(a). This curve corresponds to the frustration through the cells of $f=0.23$. In Fig. 1.4(b) the dependence of the critical current versus magnetic field is presented.

From the I-V curve of the array one can see that there are two resonances at the voltage of about $87 \mu\text{V}$ and $260 \mu\text{V}$. The frequencies of both resonances (42 and 126 GHz) are out of the working range of our receiver (78-120 GHz). We have tried to measure radiation from the array at frequencies corresponding to the harmonics of the major resonances. At the frequency of the local oscillator (LO) of about 82 GHz we succeeded to observe some radiation. The black line with triangles in Fig.1.4(a) corresponds to the measured radiation power. For the LO frequency is of 82 GHz, the radiation peaks are located near to the voltages of the lower

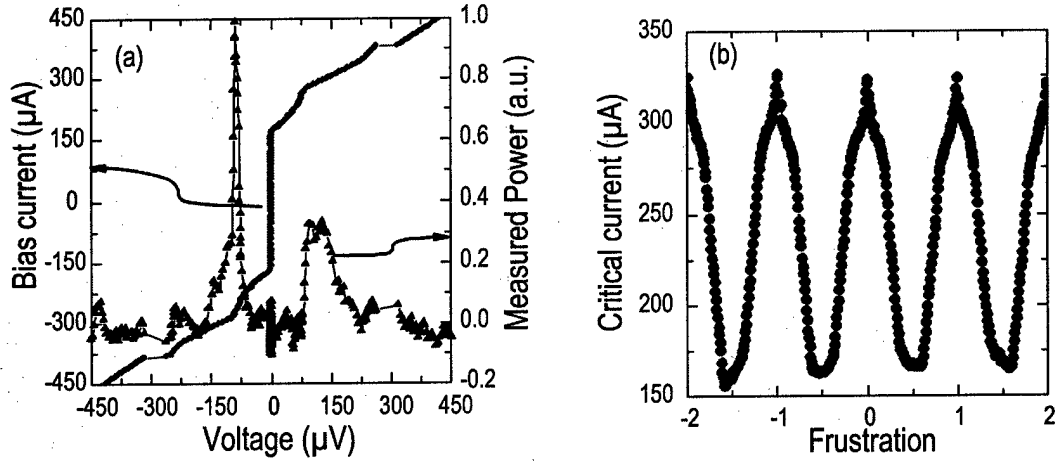


Figure 1.4: dc characteristics of the array C79#1: (a) I-V curve (dots) and measured power vs. voltage (triangles), (b) critical current vs. frustration pattern

resonance, which corresponds to 42 GHz. We believe that the detected radiation is the second harmonic of the lower resonance.

In Fig.1.5(a) we present the dependence on the frustration for the critical current (dots) and maximum measured radiation power (triangles). The power vs. frustration curve looks quite regular. From this curve we deduce that the array radiates maximum power at 82 GHz for frustration around 0.25 and 0.75. Fig.1.5(b) presents I-V curves and measured radiation power (inset) at frustration 0.23 (black symbols) and 0.78 (red line). The data corresponding to the frustration of 0.78 are asymmetric. At the positive voltages two I-V curves look the same, power vs. voltage curves are also very similar. I-V curves at the negative voltages are slightly different, consequently the measured power is also different.

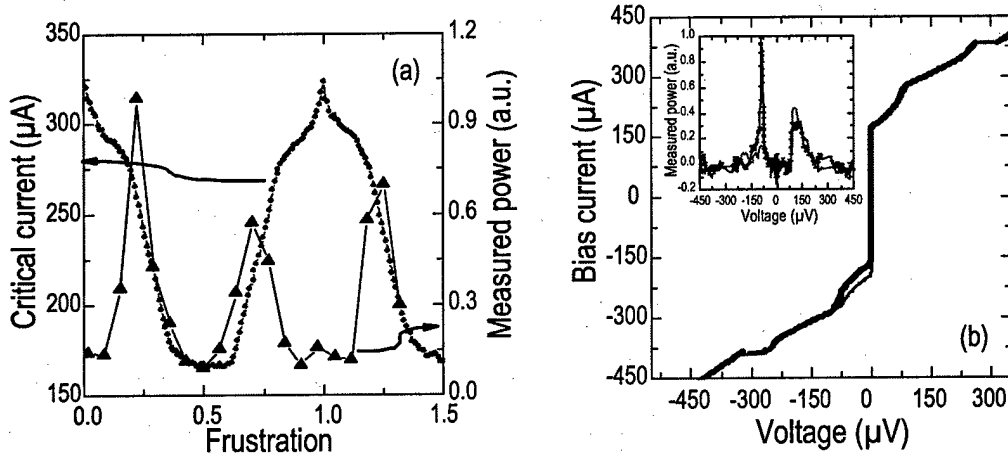


Figure 1.5: (a) Frustration dependence of the critical current (dots) and measured power (triangles) of the sample C79#1; I-V curves and measured power (inset) at frustration 0.23 and 0.78

4.2 Sample C92#2

The measurements with this array were done at a little higher temperatures (7.9 K). The measured I-V curve and $I_c(H)$ pattern are presented in Fig.1.6. On the I-V curve (dots

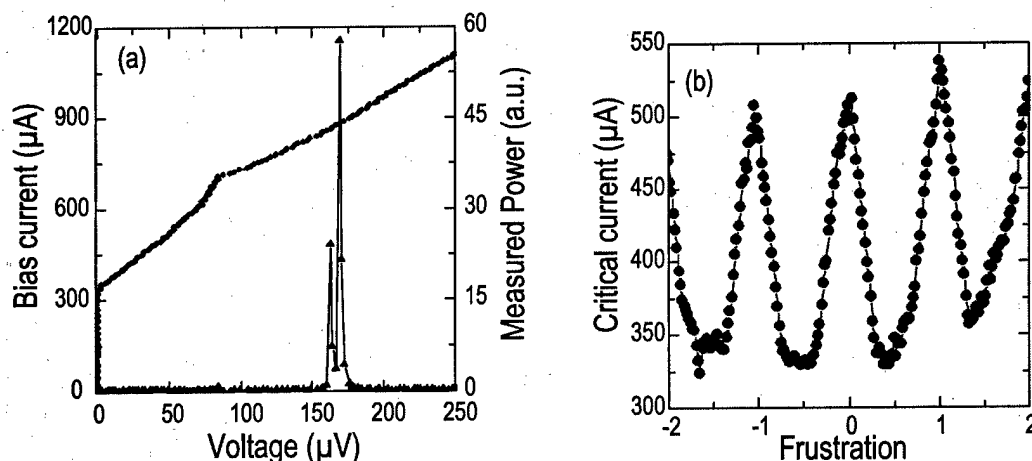


Figure 1.6: dc characteristics of the array C92#2: (a) I-V curve (dots) and measured power vs. voltage (triangles), (b) critical current vs. frustration pattern

in Fig.1.6(a)) of the array there is resonance at 85 μV . The higher resonance (which was observed at lower temperatures at voltage of about 165 μV) is suppressed at this temperature due to high dissipation. However, we were able to measure relatively strong radiation from the array close to the voltage corresponding to the higher resonance. The LO frequency was set to 80 GHz. The triangles in Fig.1.6(a) show the measured power. This curve has two sharp peaks around the voltage of 165 μV . In the Fig. 1.6(b) the dependence of the critical current versus magnetic field is presented.

In Fig.1.7 we present the critical current (dots) and the radiation power (triangles) dependence on the frustration. One can see that the radiation is at maximum at nearly half-integer frustration. Small detuning of the frustration sharply reduces radiation. The maximum measured power was about sixty times large than that of the sample C79#1. This is partially due to the fact that the main harmonics have higher radiation power and at least partially due to the larger size of the junctions of the array C92#2 and, consequently, larger dc power supplied. We suppose also that better coupling of the array to the waveguide was achieved in latter case.

Thus, from sample C79#1 we have detected radiation at frequency of 82 GHz, which corresponds to the second harmonic of the lower resonance. The largest power was detected from the sample C92#2. The frustration dependence of the measured power is found to be quite regular for all arrays.

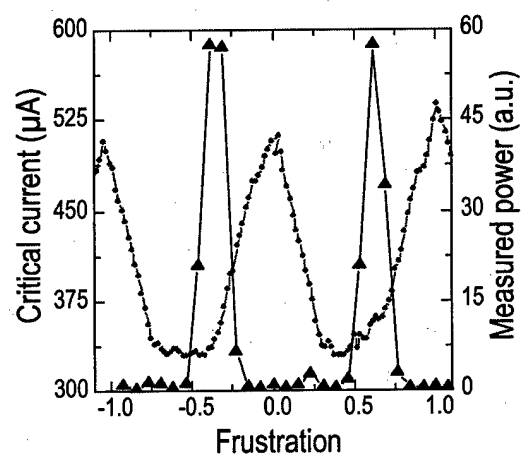


Figure 1.7: Frustration dependence of the critical current (dots) and measured power (triangles) of the sample C92#2

Bibliography

- [1] A.K. Jain, K.K. Likharev, J.E. Lukens and J.E. Sauvageau Phys. Rep. **109**, 309 (2000)
- [2] Sergey Shitov, private communication (2000)

Chapter 2

Full-wavelength loop antenna arrays

1 Loop antenna array

A Josephson junction row array, where the perimeter of each rectangular cell in the row of about one wavelength, may provide a simple way to achieve a phased array sub-mm radiation source. The beam formed above the array may be directed by imposing a uniform external magnetic field over the whole array and thereby inducing a constant phase shift in the emitted radiation from cell to cell. The main concern with this type of array is that due to fabrication defects, the spread in the DC voltages (and consequent frequencies) of the contributing junction oscillators may overwhelm the contribution of the oscillating antenna current that tends to keep the junction oscillators in synch. Preliminary calculations by S. Yukon and F. Lin indicate that when the junctions are matched to the antenna impedance, these currents can be significant and may allow such a system to work [1]. In Fig. 2.1 we present electric scheme of single (a) and double (b) cell arrays with 4x5 Josephson junctions per cell.

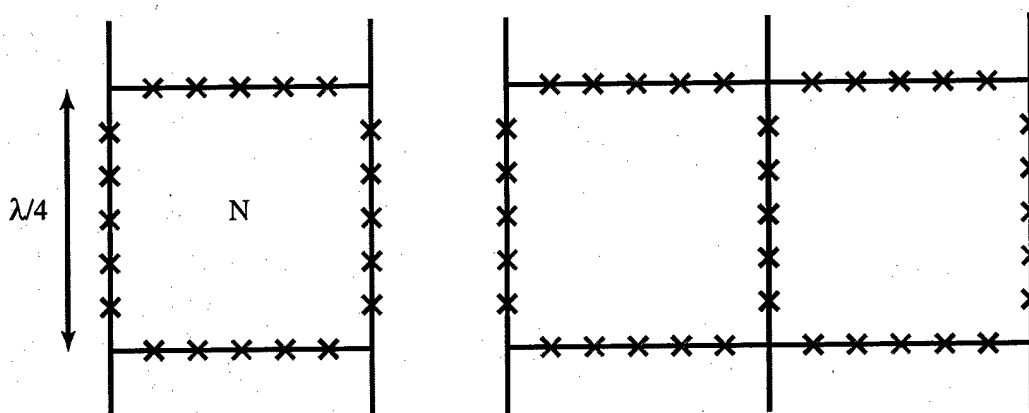


Figure 2.1: Equivalent scheme of a loop antenna array with one (a) and two (b) cells

2 Measurements and discussion

According to our layout and specification, the samples having the critical current density $J_c \simeq 1000 \text{ A/cm}^2$ were prepared at the foundry HYPRES [2]. The samples are single cell or double cell arrays. The arrays are with 4x3, 4x4, 4x5, 4x6 and 4x7 around a cell. The size

of each junction is about $9 \mu\text{m}^2$. Fig. 2.2 shows a micro photograph of the sample #34-1x4x5. Table 2.1 presents all specific parameters of the prepared samples. The inductance was estimated using numerical results by Ketchen [3].

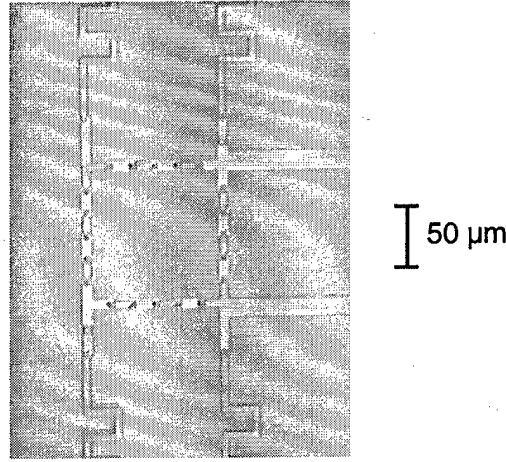


Figure 2.2: Micro photograph of the sample #34-1x4x5, loop antenna array with 4x5 junctions

Table 2.1: Estimated parameters of the samples

Number of junctions	Cell size, μm^2	Total capacitance, fF	Cell inductance, pH	Resonance frequency, GHz
4x3	4356	30	147.6	75.6
4x4	7056	22.5	194.2	76.1
4x5	10404	18	249.9	75.0
4x6	14400	15	301.6	74.8
4x7	19044	12.9	355.5	74.3

The layout of a single cell array with 4x5 junctions is presented in Fig. 2.3. The external bias current (I_{bias}) is injected at each node of the array via 67Ω resistor (along the vertical direction in Fig. 2.3) and voltage (V) is measured across the vertical junctions. The description of the used measurement setup can be found in one of our previous reports [4].

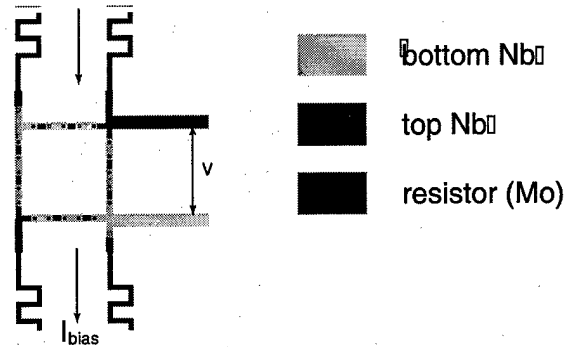


Figure 2.3: Layout of a cell with 4x5 junctions

We have measured current voltage (I-V) characteristics of the arrays at the temperature range 4.2-8 K. Due to their large inductance the arrays are insensitive to external magnetic

field perpendicular to the array plane.

In Fig. 2.4 we present several I-V curves of single loop arrays taken with storage oscilloscope at different temperatures. I-V characteristics of double cell arrays taken at different temperatures are presented in Fig. 2.5.

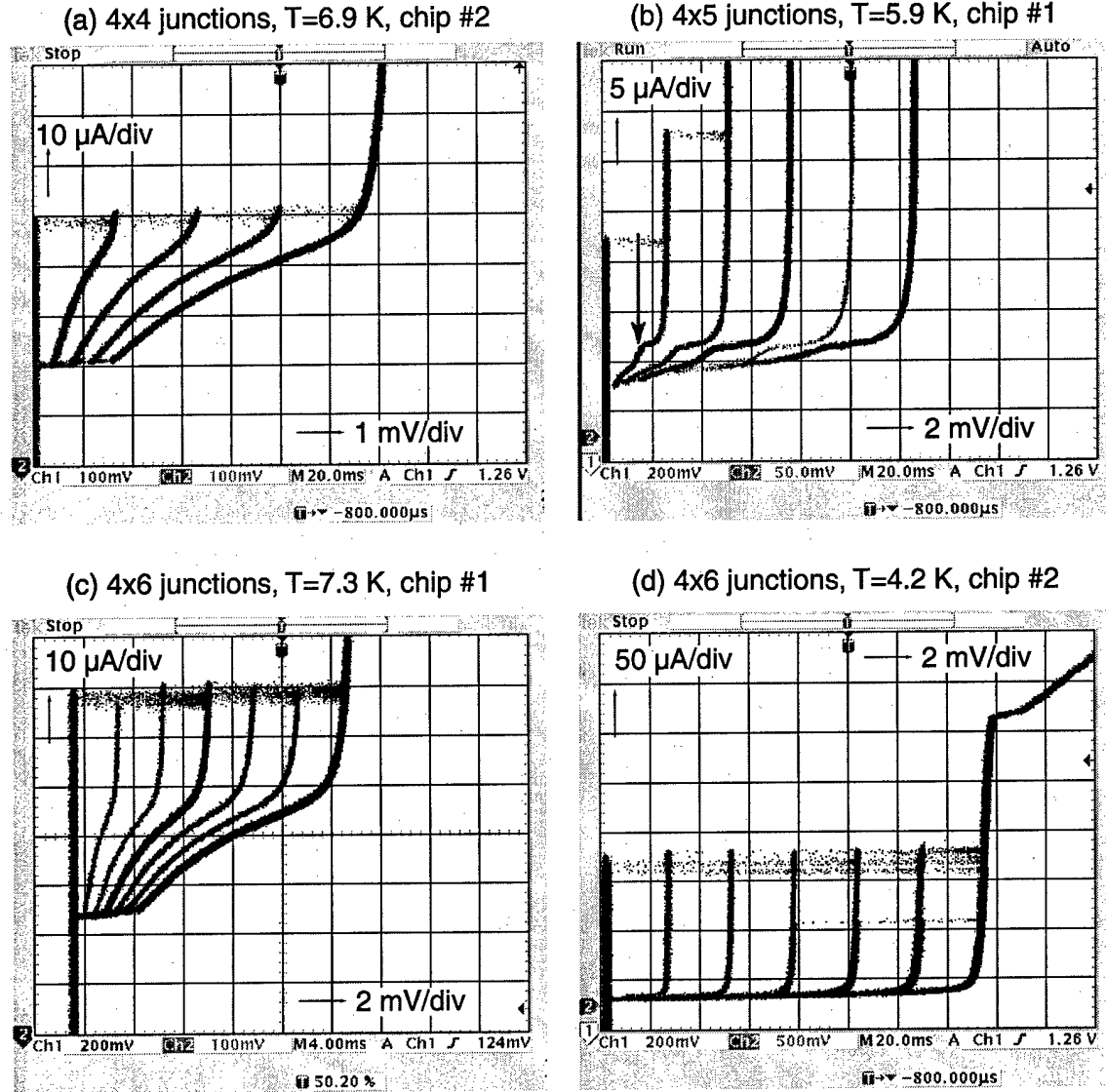
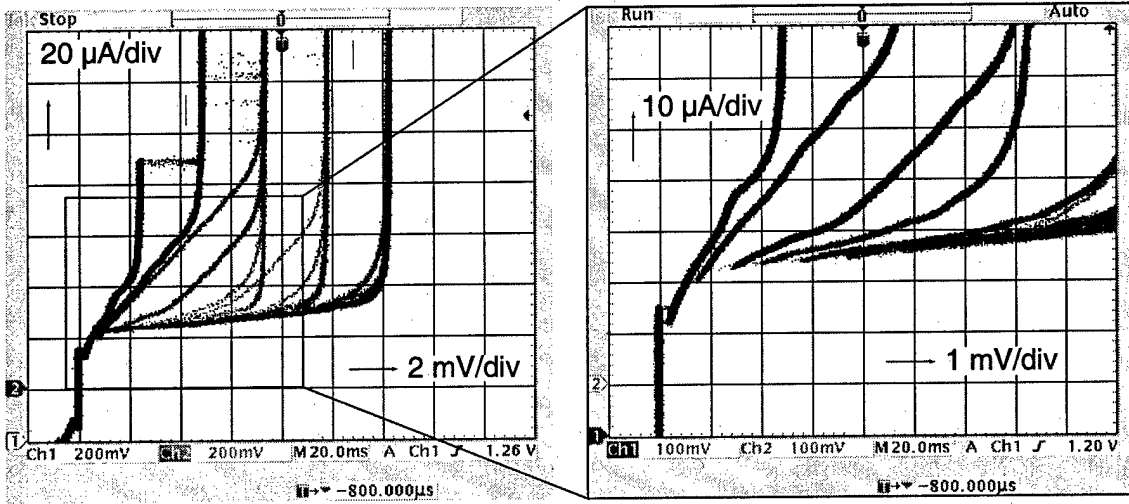


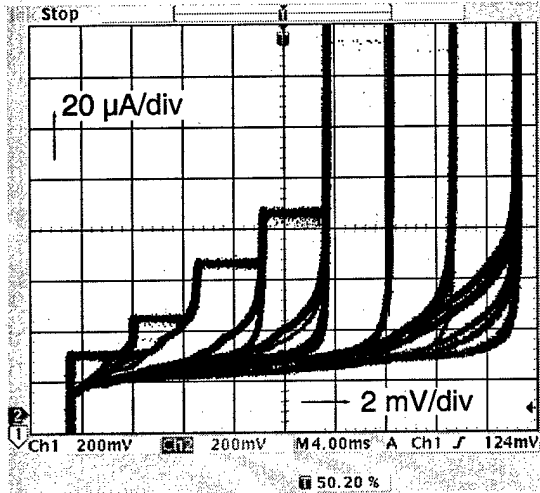
Figure 2.4: I-V characteristics of single cell arrays with 4x4 (a), 4x5 (b), 4x6 (c) and 4x7 (d) junctions around a cell

Fig. 2.4(a) presents I-V characteristics of a cell with 4x4 junction measured at $T=6.9$ K. From this figure we note that all of four vertical junctions switch to resistive state at nearly the same bias current. However, in spite of their small spread we could measure all the resistive branches. To measure n-th branch we increase (decrease) bias current until the system switches to this state and decrease (increase) it until the system switches to another branch. On this I-V curve we find no resonance branches. We did not observe any resonance in the whole temperature range that we measured.

(a)-(b) 4x5 junctions, $T=4.5$ K, chip #2



(c) 4x7 junctions, $T=4.5$ K, chip #2



(d) 4x7 junctions, $T=4.2$ K, chip #1

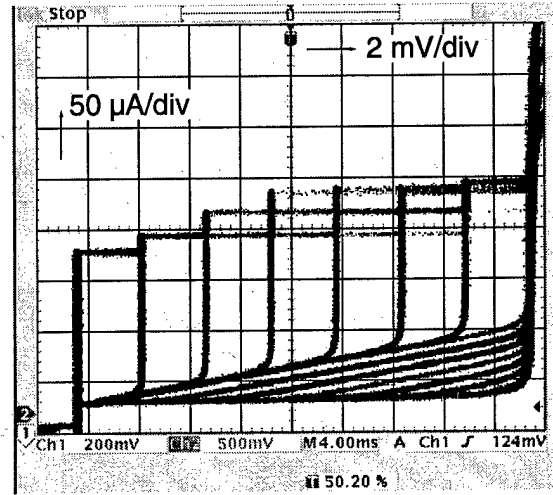


Figure 2.5: I-V characteristics of double cell arrays with 4x5 (a)-(b) and 4x7 (c)-(d) per cell

Fig. 2.4(b) shows I-V curve of a cell with 4x5 junctions at $T=5.6$ K. This sample shows some resonance behavior. The first resonance step (indicated by red arrow in Fig. 2.4(b)) appears at frequency about 710 GHz, which is much higher than the expected frequency (~ 75 GHz). The same steps can be seen at the bottom part of all branches. One can also see that the critical currents of different branches are different, so that the sample is not uniform and it is hard to interpret its behavior.

Fig. 2.4(c) presents I-V curve of a single cell array with 4x6 junctions. The measurement were done at temperature 7.3 K. This sample shows nearly the same critical current of different branches. n -th branch corresponds to the state with n vertical junctions are in resistive state. We also did not observe any resonance with this sample.

The I-V curve presented in Fig. 2.5(d) corresponds to 2 cell array with 4x7 junctions per cell. The first 6 branches are similar to that of a single cell array. However, the 7-th branch

itself splits to other 7 branches. In order to measure them we increased bias current until some value (we denote it as I_{stop}) and then decrease it until zero. Depending on I_{stop} different branches appear on the I-V curve. We believe that they correspond to different configurations of several horizontal and vertical junctions in resistive state. Such states are called discrete rotobreathers and have been observed in Josephson ladder arrays [5, 6].

We have measured more than 15 different arrays. All arrays with single cell show similar behavior like in Fig. 2.4(a)-(c). This corresponds to one by one switching to resistive state of vertical junctions. The arrays with two cells have more complicated dynamics. They show different branches not only at the bottom part of the last gap, but also at the bottom parts of other gap branches.

3 Conclusion

Measurements with full wave length loop antenna arrays have been performed. We did not observe any systematic resonances. All of the single cell arrays have shown more or less uniform critical current of different branches on the I-V curve. The arrays with 2 cells have shown different breather states. In order to investigate exactly which junctions are in the resistive state at the given voltage one may make additional probes to measure voltages across each junction. An easier possible method is using our low temperature scanning laser microscope [6].

Bibliography

- [1] Stanford Yukon, private communication (2000)
- [2] <http://www.hypres.com>
- [3] M.B. Ketchen, IEEE Trans. Magn. **MAG-23**, pp.1650-1657, (1987)
- [4] A.A. Abdumalikov, P. Caputo and A.V. Ustinov, Interim Report No. 1 on Testing of Josephson array antennas and trim currents tuning, contract F61775-00-C0004
- [5] E. Trias, J.J. Mazo, A. Brinkman and T.P. Orlando, Physica D **156**, pp. 98-138, (2001)
- [6] P.Binder, D. Abraimov, A.V. Ustinov, S.Flach and S. Zolotaryuk, Phys.Rev.Lett. **84**, pp. 745-748, (2000)

Chapter 3

Replacement of resistors by Josephson junctions in biasing leads

1 Introduction

The conventional biasing scheme of Josephson junctions arrays consist of resistor network (Fig.3.1a). In order to have a homogenous bias current over the whole array, the resistances in the biasing have to be large in comparison with junction sub-gap resistance. Such resistors extend over several cell lengths from the array and may decrease the radiation efficiency.

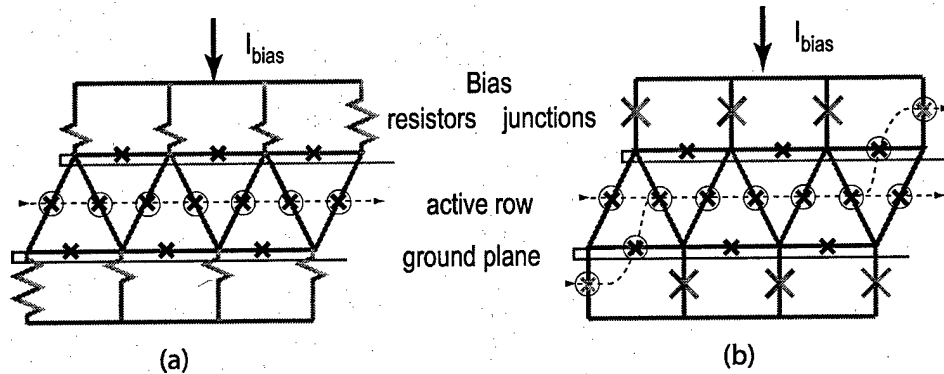


Figure 3.1: Schematic top view of the arrays with resistor biasing (a) and junction biasing (b) networks. Red junctions belong to active oscillator row, while green junctions form the bias network. Dashed lines show the possible flux flow direction through the arrays.

Following recent proposal by Stanford Yukon [1], we have replaced the bias resistors by Josephson junctions (Fig. 3.1b). According to theoretical calculations, the radiation efficiency is supposed to be around 3-4% larger than that of arrays with resistive biasing. Because the bias junctions are supposed to switch to the resistive state at a current *equal or less* than the switching current of the vertical junctions in the active row, one may neglect the Meissner state in the biasing network.

In case of resistive bias, the resistor connected to the corner vertical junction is twice larger than resistors connected to two vertical junction. Following this idea, the bias junction connected to only one vertical junction should be twice smaller than the bias junction supplying current to two vertical junctions of the active array.

2 Array layout

The design of the arrays schematically shown in Fig. 3.1 was based on our previously studied arrays [2]. The active row junctions have an area of $9 \mu\text{m}^2$ and the cell size is $150 \mu\text{m}^2$. The junction area of $9 \mu\text{m}^2$ is close to the smallest permitted by the Hypres design rules and we decided to keep it unchanged from the previously made and tested design. The bias network have junctions with an area of $18 \mu\text{m}^2$ (edge junction of $9 \mu\text{m}^2$). The total area (and thus, the field-free critical current) of each of the bias rows is equal to that of the active row. Thus, at zero frustration and absence of self-field effects all rows are supposed to switch to the resistive state at the same bias current.

In order not to affect the resonance properties of the active row the bias cell size was chosen much larger than the size of active row cells. We have designed arrays with two different cell size, $3000 \mu\text{m}^2$ (sample #1) and $700 \mu\text{m}^2$ (sample #2). As a reference array we have put an array with resistor-based biasing (reference sample). The resistors are about 25Ω (edge resistor $\sim 50 \Omega$). All designed arrays have 12 cells in the active row. All horizontal junction are embedded into a stripline formed between the array electrodes and the ground plane below them.

3 Experimental results

According to our design, the samples were fabricated at Hypres foundry. The critical current density of the junctions is about 1000 A/cm^2 at 4.2 K. All measurements were done at 7.9 K. We have systematically measured current-voltage characteristics and perpendicular magnetic field $I_c(H)$ pattern of the critical current and the resonance voltage.

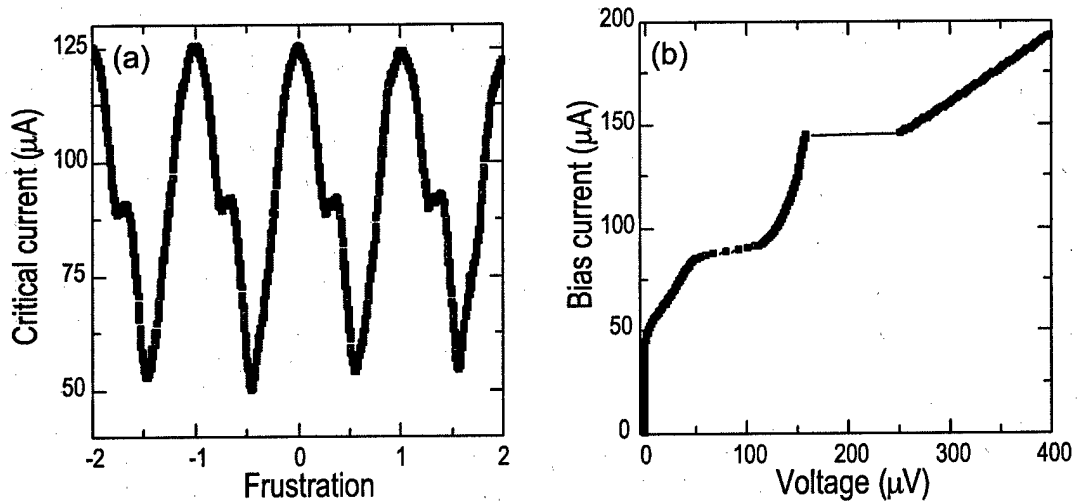


Figure 3.2: Magnetic field pattern of the critical current (a) and current-voltage characteristics at $f=0.3$ (b) of the array with resistor based bias network.

In Figure 3.2a we present $I_c(H)$ pattern of the reference array with biasing via resistors. As expected, we find regular oscillations of the critical current. Its current voltage characteristics at frustration $f=0.3$ shows well pronounced resonance at voltage of about $170 \mu\text{V}$.

The dependence of the critical current of the active row of sample #1 is shown Fig. 3.3a. For comparison, we present the $I_c(H)$ pattern of the bias row in Fig. 3.3b. In spite of the regular oscillation of the bias rows' critical current, the critical current of the active row is

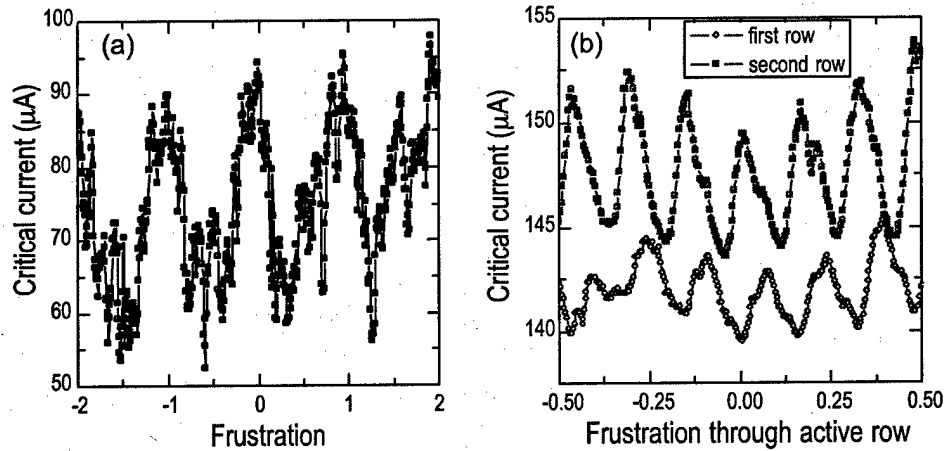


Figure 3.3: Magnetic field patterns of the critical current of the active row (a) and of the bias rows (b) of the array with junction-based biasing. Biasing cell size is $3000 \mu\text{m}^2$.

rather irregular. Note, that in order to exclude possible effects of residual fields the reference array was measured in the same run as samples with junction-based biasing network. Second peculiar point is that the active row critical current is smaller than that of biasing rows. The ratio of the oscillation periods of the bias rows and active row is about three times smaller than the ratio of the corresponding cell sizes. The critical currents of the bias row also differ from one another.

The I-V curve of sample #1 is presented in Fig. 3.4 at frustration $f=0.4$. The I-V curve of the active row is similar to that of the array with resistive biasing. The I-V curve of the second biasing row (red symbols) shows a small peculiarity by deviating from zero voltage state at bias current of about $90 \mu\text{A}$. This biasing row remains in the resistive state up to the current $I_{\text{bias}}=110 \mu\text{A}$ and then returns back to the superconducting state.

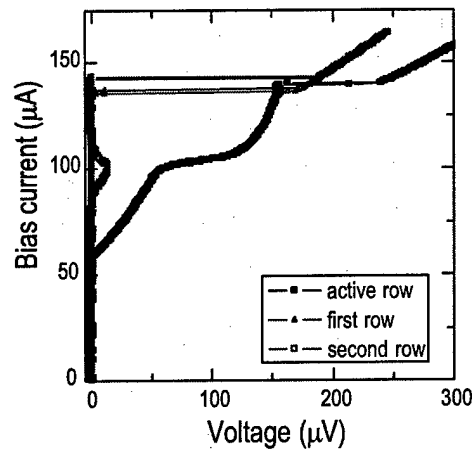


Figure 3.4: Current voltage characteristics of the array with junction based biasing. Biasing cell size is $3000 \mu\text{m}^2$.

This peculiar reentrant behavior has been previously observed by us for symmetry-broken states in Josephson junction arrays. It's spatial patterns have been visualized by using low temperature scanning laser microscope [4, 5]. Possible explanation for the array dynamics in

the measurements presented here is illustrated in Fig. 3.1. The junctions marked by circles are in resistive state and the dashed line shows how the magnetic flux travels across the array. Thus, symmetry-broken states occur when one or more horizontal junctions (placed in the direction perpendicular to the bias current) go resistive.

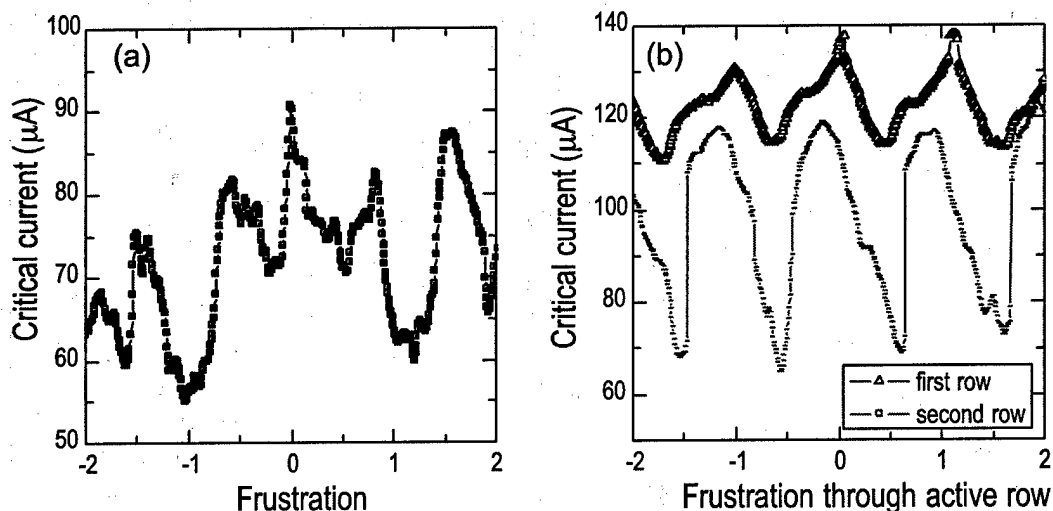


Figure 3.5: Magnetic field patterns of the critical current of the active row (a) and of the bias rows (b) of the array with junction-based biasing scheme. Biasing cell size is $700 \mu m^2$.

The dependence of the critical current of the active row of sample #2 is shown Fig. 3.5a and the $I_c(H)$ pattern of the bias rows in Fig. 3.5b. These patterns are similar to that of sample #1. The ratio of the areas of the cells in the biasing and active rows is about 4. However, the oscillation period of the critical current of the bias rows is same as that in the active row.

The I-V curves the array #2 (Fig. 4.4, $f=0.7$) are similar to the I-V curve of the sample #1. The peculiar reentrant resistive state appears now for both bias rows (red and blue symbols), but at different bias currents.

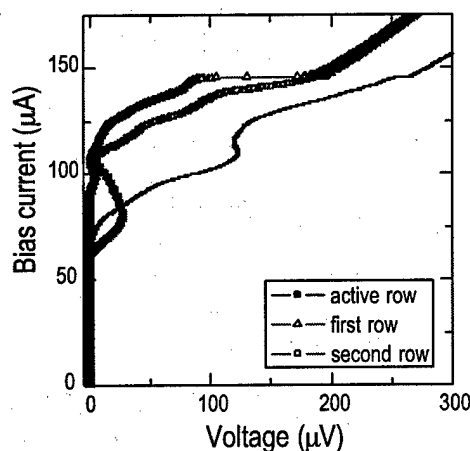


Figure 3.6: Current-voltage characteristics of the array with the junction-based biasing scheme. Biasing cell size is $3000 \mu m^2$.

Finally, by biasing arrays at constant bias current, we have measured the magnetic field patterns of the voltage at the resonant step. In Fig.3.7 we present $V(H)$ patterns at $I_{\text{bias}} = 120 \mu\text{A}$ for the all three arrays are presented. Similar to critical current patterns, the $V(H)$ patterns of the arrays with junction biasing are irregular.

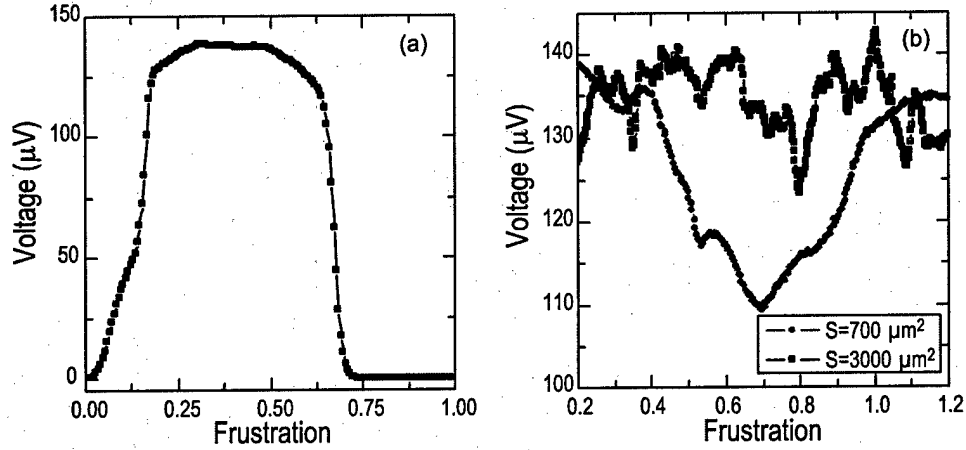


Figure 3.7: Volt-field pattern of the reference array (a) and of the arrays with junction-based biasing scheme (b).

4 Conclusion

We have experimentally studied the array of Josephson junctions with biasing via a row of Josephson junctions. We have observed that, in the operational range of frustration, the active oscillator row switches to the resistive state at lower current, at which biasing junctions are still in the superconducting state. We also find strong unwanted dynamic interaction between the oscillator and biasing rows of junctions. This dynamic interaction most probably corresponds to symmetry broken states.

The area (and thus the critical current) of biasing junctions in this layout was limited by Hypres design rules. In principle, by modifying the design of our standard oscillator to larger junctions we should be able to make biasing junctions switching before the active row. This would require additional test run in order to vary the modified cell sizes and match the radiation frequency range of the receiver at 80-120 GHz. Nevertheless, we suppose that the *dynamic* interaction between the oscillator and the biasing rows will remain a serious problem in such a design.

Bibliography

- [1] Stanford Yukon, private communication (2002)
- [2] P. Caputo and A.V. Ustinov, Iterim report on "Analysis of Triangular Arrays of Josephson Tunnel Junctions", contract F61775-01-W-E041 (1998)
- [3] <http://www.hypres.com>
- [4] D. Abraimov, P. Caputo, G. Filatrella, M. V. Fistul, G. Y. Logvenov, and A. V. Ustinov, Phys. Rev. Lett. **83**, 5354 (1999).
- [5] P. Binder, D. Abraimov, A. V. Ustinov, S. Flach and S. Zolotaryuk, Phys.Rev.Lett. **84**, pp. 745-748, (2000)

Chapter 4

Triangular prism qubits

1 Introduction

Several novel qubit devices have been proposed by Stanford Yukon [1, 2]. The most intriguing of these is a discretized version of the triangular long Josephson junction prism [3-7]. Currently, there is no technical method to make such a real 3D system. There has been proposed [8] a flattened 2D version of the qubit, which is shown in Fig. 4.1. Potential energy profile of this qubit is periodic and each period has two minima. These minima of

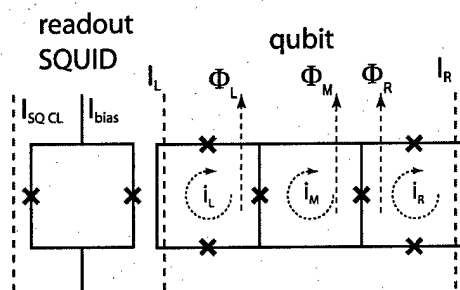


Figure 4.1: 2D version of Yukon's qubit and a read-out SQUID.

the potential profile of this system are associated with the circulating current in the left ($i_L = I_{\min}$, $i_R = 0$) and right loops ($i_L = 0$, $i_R = I_{\min}$). The flux Φ_M and $\Phi_L + \Phi_R$ determine the barrier height. With change of barrier height its the width of the wells and of the barrier and I_{\min} change. By changing the differential flux ($\Phi_L + \Phi_R$) between the flux through the left and right loops one can make the potential profile asymmetric. The qubit state can be measured with help of read-out SQUID placed next to it.

The standard qubit based on the single-loop SQUID has a double well potential at half frustration and relies on the external field. The important feature of the Yukon's qubit is that it should be less sensitive to fluctuations of the external magnetic field. Another interesting property of this qubit is that the barrier height can be changed without changing the symmetry of the potential profile. The main difference between multi-qubit circuit based on the Yukon's qubits and single-loop qubits is that former ones can be coupled by Cirac-Zoller type of bus. [9]

2 Design

In order to characterize the potential energy profile in the classical regime, we have made design of the circuit shown schematically in Fig. 4.1. There are several constrictions for the parameters of the qubit and dc-SQUID. These constrictions are set by the design rules of the foundry [10].

In the theoretical calculations the qubit cell inductance is neglected. However, technological processes put the lower limit on the size of cell. In order to minimize the cell inductance of the qubit we made the cell size $2 \times 2 \mu\text{m}$. The roughly estimated inductance of the cell is about $L = 3 \text{ pH}$. The junction size is about $3 \times 3 \mu\text{m}$.

For making standard current-biased SQUID read-out, the junctions of the SQUID should be overdamped and its β_L parameter should be of the order of one. In order to have an overdamped case, junctions were shunted by a resistance of 5Ω . The cell size of the SQUID was made $8 \times 8 \mu\text{m}$. The layout is shown in Fig. 4.2.

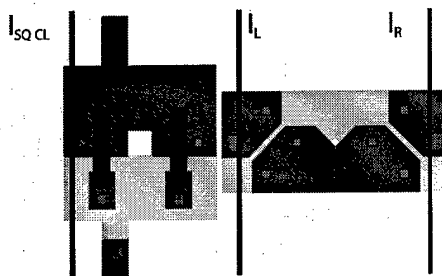


Figure 4.2: Design layout

A magnetic flux through the SQUID cell is controlled by a current through the control line (CL) marked as $I_{SQ CL}$. The qubit state is controlled by currents through CLs marked as I_L and I_R . Unfortunately, the circuits designed with a middle CL (for applying differential flux) came defected from the foundry due to a limitation given by design rules. Samples either with or without ground plane were designed on the chip.

3 Experiment

Samples according to our micro design were prepared at Hypres foundry. The critical current density was about 1000 A/cm^2 at 4.2 K . In spite that the junctions were shunted, the read-out SQUID was slightly in a hysteretic regime. In order to make it sufficiently overdamped we have increased temperature up to 5 K . As expected, the samples with the ground plane were almost insensitive to the fields produced by CLs for currents up to 50 mA .

First, we have characterized the read-out SQUID. In Fig. 4.3 we present the measured current-voltage characteristics (a) and critical current versus frustration produced by $I_{SQ CL}$ (b). From this curves we have estimated the SQUID's parameters as $\beta_L = 2.66$ and $\beta_C = 0.25$.

As a working point of the read-out SQUID we have chosen the bias current and frustration with largest dV/dI and dI_c/df_{SQ} response amplitudes. This point is marked by a solid dot on I-V curve ($I = 164 \mu\text{A}$) and $I_c(H)$ pattern ($f_{SQ} = 0.75$). We have fixed the current I_R through the right CL while sweeping the current of I_L the left CL and measuring the voltage of the SQUID. In Fig. 4.4 we present voltage-field curves corresponding to increase of frustration (black line) and decrease of frustration (red line) for $I_R = 153 \mu\text{A}$. The inset presents the difference between this curves. The differential flux between the left and right loops vanishes ($\Phi_L = \Phi_R$) at $I_L = 153 \mu\text{A}$ ($f_{SQ} = 0.2$).

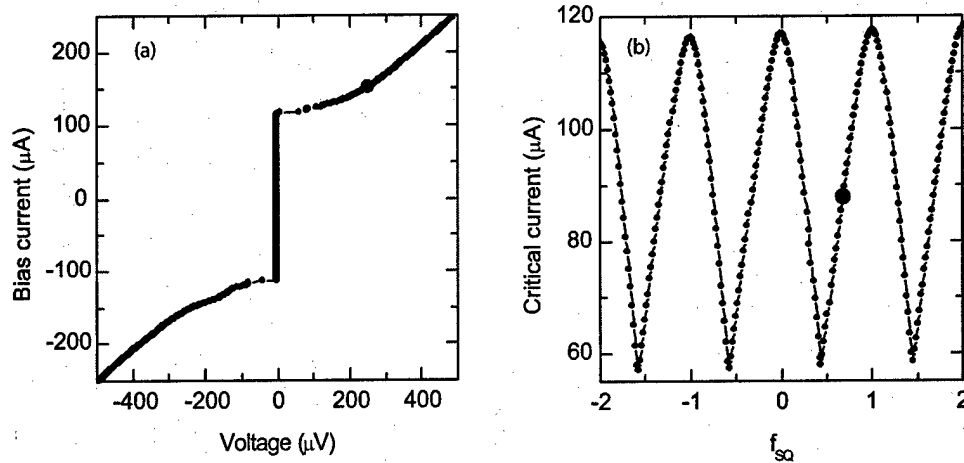


Figure 4.3: Current-voltage characteristics (a) and critical current pattern vs. frustration (b) of the read-out SQUID

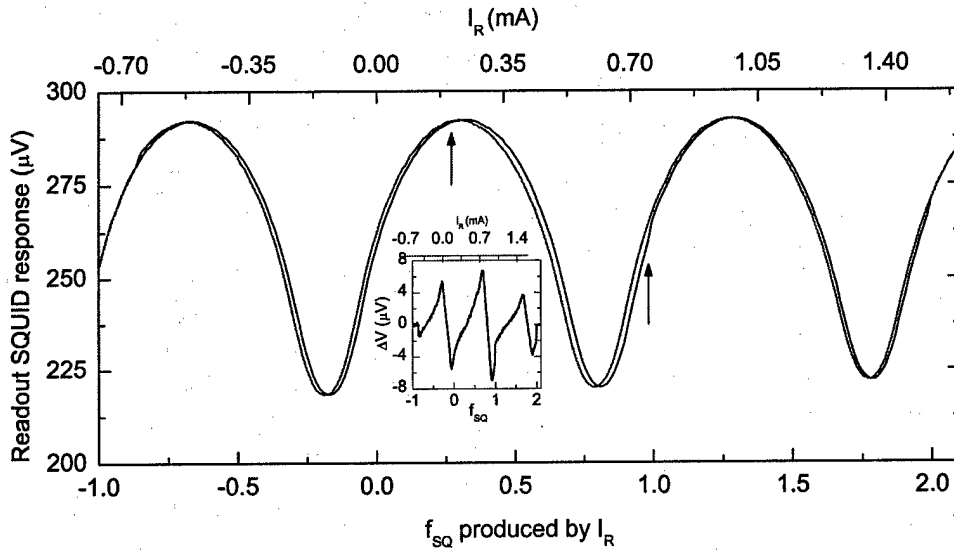


Figure 4.4: Read-out SQUID response to increase (black line) and decrease (red line) of current I_L . Inset: the difference between the two curves.

The hysteresis shown in Fig. 4.4 starts at $f_{SQ} \simeq -0.86$. At $f_{SQ} \simeq 0.3$ (red arrow) it abruptly increases and again decreases at $f_{SQ} \simeq 1.0$ (black arrow). The hysteresis vanishes at $f_{SQ} \simeq 1.98$. The effective change of the frustration through SQUID for larger hysteresis is about $\Delta f \simeq 15.3 \times 10^{-3}$ and for smaller one it is $\Delta f \simeq 8.7 \times 10^{-3}$. We suppose that large hysteresis occurs due to a switch of the system between the left (Fig. 4.5a) and the right (Fig. 4.5b) minima.

The smaller hysteresis occurs due to change of sign of a mesh current in one of the qubit cells. For example, between states shown in Fig. 4.5b and Fig. 4.5c the mesh current i_R changes its direction. In order to better understand the double-hysteretic behavior we plan to perform another experiment with CLs which change the flux differentially and/or change

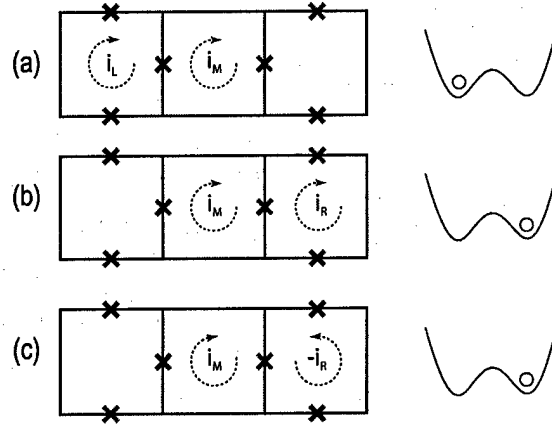


Figure 4.5: For explanation of two hysteresis: a) system is in the left minimum; b) system is in the right minimum; c) system is in right minimum, but with a negative mesh current.

the total flux through left and right loop, leaving the flux in the middle loop unchanged.

4 Conclusion

We have performed first experiments with novel Josephson junction qubits. We have observed that the read-out response has a double-hysteretic behavior. Next step will be to investigate this hysteresis in dependence on the second control line current and to find out the magnetic field periods of the qubit by its dc characterization. We note several design improvements to be made. First, we have to improve the coupling of our read-out system. Next, a differential flux control line has to be added. It planned to develop an improved version of this layout in the near future.

Bibliography

- [1] S.P. Yukon, *Physica C* **368**, 320 (2002)
- [2] S. P. Yukon, private communication (2000)
- [3] S.P. Yukon, N.C.H. Lin, *IEEE Trans. Mag.* **27**, 2736 (1991)
- [4] S.P. Yukon, N.C.H. Lin, in *Nonlinear Superconducting Devices and High- T_c Materials*, edited by R.D. Parmentier and N.F. Pedersen (World Scientific, Singapore, 1995)
- [5] S.P. Yukon, N.C.H. Lin, in *Macroscopic Quantum Phenomena and Coherence in Superconducting Networks*, edited by C. Giovanella and M. Tinkham (World Scientific, Singapore, 1995)
- [6] S.P. Yukon, N.C.H. Lin, *IEEE Trans. Appl. Supercond.* **5**, 2959 (1995)
- [7] G. Carapella, G. Costabile, P. Sebastino, *Phys. Rev. B* **59**, 14040 (1999)
- [8] S. P. Yukon, private communication (2001)
- [9] J.I. Cirac, P. Zoller, *Phys. Rev. Lett.* **74**, 4091 (1995)
- [10] <http://www.hypres.com>

Chapter 5

Declarations

(1) The Contractor, Prof. Dr. Alexey Ustinov, hereby declares that, to the best of its knowledge and belief, the technical data delivered herewith under Contract No. F61775-01-WE045 is complete, accurate, and complies with all requirements of the contract.

(2) I certify that there were no subject inventions to declare as defined in FAR 52.227-13, during the performance of this contract.

DATE: April 2, 2003

Name and Title of Authorized Official:

Alexey Ustinov, PhD
Professor of Experimental Physics
University of Erlangen-Nuremberg, Germany